Roughening transitions and surface tension in an hcp lattice with higher neighbor interactions

Adham Hashibon, Joan Adler, Gideon Baum, and S. G. Lipson
Department of Physics, Technion-IIT, 32000 Haifa, Israel
(Received 10 February 1998)

We report on Ising lattice-gas simulations of surfaces of a hexagonal-close-packed (hcp) crystal as a function of temperature and higher neighbor interactions using sample sizes up to $160\times160\times40$ sites. The hcp lattice represents ^{4}He on which three roughening transitions have been observed experimentally. Most previous simulation studies on roughening transitions were performed for other lattices where fewer experimental data are available. We calculated roughening temperatures for these three surfaces as a function of higher neighbor interactions of both signs. We also calculated the surface tension of the three facets. In most cases good qualitative (and reasonable quantitative) agreement with experiment was found with appropriate values of interactions, confirming the basic validity of the model as applied to surface roughening.
[S0163-1829(98)03831-4]

I. INTRODUCTION

The roughening transition (RT) is a phase transition that corresponds to a morphological change in the interface between a crystal and its fluid or vapor in thermal equilibrium. At the temperature T_R at which the RT occurs there is a singularity in the interfacial tension. We can define an intrinsic width d_w associated with the interface; this is the thickness of a surface layer over which the local physical properties change from those of fluid to solid. Thermal excitations cause local interface fluctuations, so the interface may wander over a characteristic length w. If $w\sim d_w$ the interface is called ''smooth'' but if $w\to\infty$ in the strict thermodynamic limit, the interface is called ''rough.''

The concept of the RT arose in the context of an abstract crystal-growth model put forward by Burton, Cabrera and Frank[1] (BCF) in 1951. They made an analogy between a crystal/fluid interface and a lattice populated by up and down spins. In the analogy, one direction corresponds to atoms of the solid, and the other to a vacant site, or a site filled by fluid. The interface in a $d=3$ Ising model between two regions of spins mostly up and mostly down approximates a $d=2$ surface at low temperature. In the BCF model the growing layer is described by a $d=2$ Ising model with $T_R\sim T_c(d=2)\sim\frac{1}{2}T_c(d=3)$. The basic model of BCF, though naive, gives surprisingly good numerical estimates of T_R, and in fact can be shown to provide a rigorous lower bound to T_R.[2] But the RT and the phase transition of the $d=2$ Ising model are, of course, of a completely different nature and therefore a more appropriate model for the study of a crystal in equilibrium with its fluid or vapor is the $d=3$ Ising model, again with up and down spins corresponding to fluid and solid sites. Also appropriate are solid-on-solid (SOS) models that are within the universality class of the Kosterlitz-Thouless (KT) transition;[3] they resemble Ising interfaces except that no holes or overhangs are present and give similar critical results for cubic systems.[4,5]

About 17 years ago the first equilibrium roughening transition on ^{4}He crystals was experimentally confirmed.[6] Helium is especially suited to experimental work on RT's because equilibrium between the solid and superfluid at the interface is achieved on the time scale of seconds or minutes for crystals that are large enough to be observed with suitable optical techniques. To date three roughening transitions on hcp ^{4}He have been seen: The first two facets appear[6,7] in the (0001) or **c** direction at $T_R(\mathbf{c})=1.28$ K. The six facets in the directions equivalent to $(1\bar{1}00)$ or **a**, start emerging[8] at $T_R(\mathbf{a})\sim1.0$ K. Finally, 12 $(1\bar{1}01)$ or **s** facets have been observed during growth[9] at about $T_R(\mathbf{s})\sim0.35$ K. A set of pictures of the roughening of the **a** facet from Ref. 10 is shown in Fig. 1.

In Table I, both experimental and computational measurements for the hcp lattice roughening temperatures are given. Despite the fact that the best RT data were measured on an hcp crystal most analytic and numerical work continued to be carried out on cubic crystals without further neighbors. An exception was the study of Touzani and Wortis[11] (TW), who developed exact and mean-field results for hcp models of the BCF type. When comparing ratios of their T_R values to the experimental ratios, problems are observed with the T_R of the **s** facet (see Table I). While the ratio of T_R for the **c** facet with T_R for the **a** facet is within less than 20% of the measured ratio, ratios including the **s** facet are more than 50% off. Given the uncertainty in the **a** and **s** measurements, 20% is not too bad, but 50% is obviously excessive. Several reasons for this discrepancy were proposed, including (i) lack of further neighbor interactions, (ii) lack of quantum effects, (iii) problems with the BCF-type approximation, (iv) problems with the basic idea of lattice models for RT's, or (v) experimental problems associated with equilibration in Ref. 9.

We began a comprehensive program to develop models on hcp lattices in an attempt to understand whether the disagreement between the **s**-facet experiments and simulations is fundamental or resulted from inadequate computational or experimental techniques. We started by developing a SOS model that maps to a 12-vertex model for the **c** facet. Unfortunately, this model does not appear to have an exact solution. In general, however, a full three-dimensional Ising spin system was found to be easier to simulate than SOS models

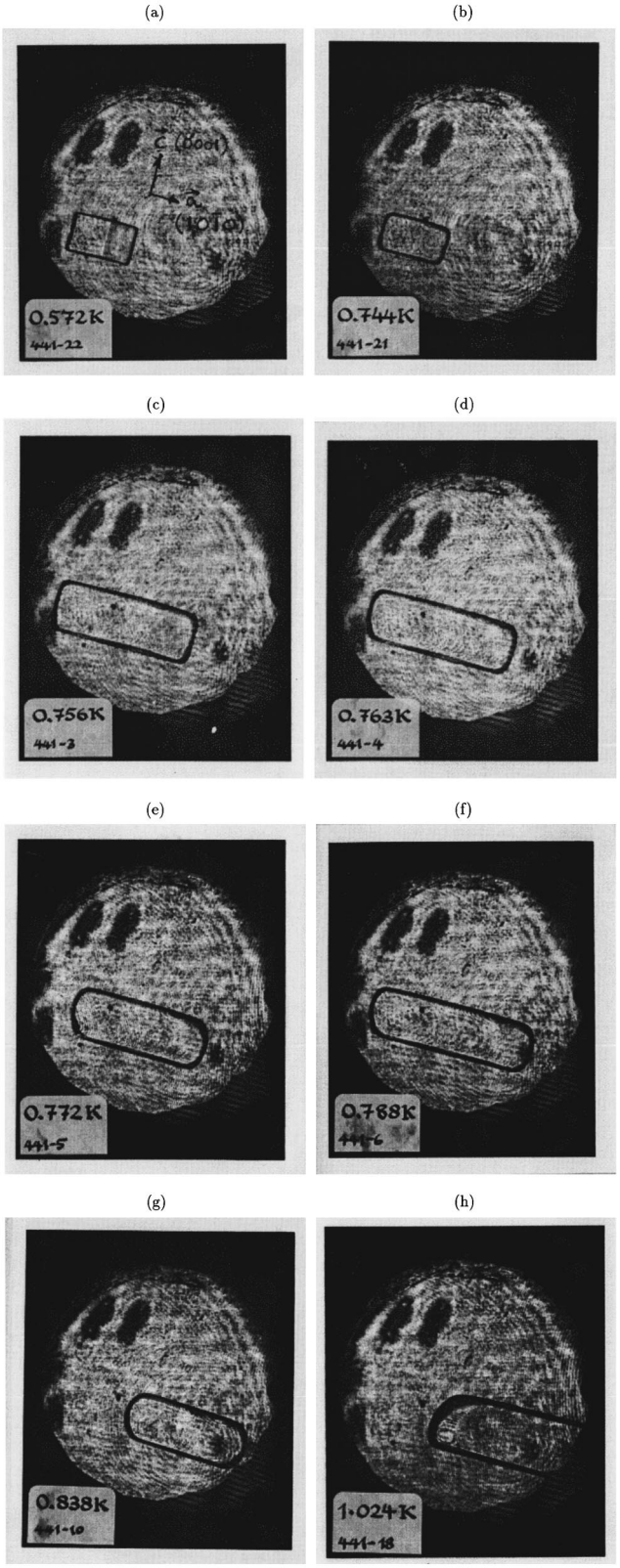

FIG. 1. The history of a $(1\bar{2}10)$ hexagonal crystal of helium in a superfluid helium environment warmed very slowly. Each photograph was taken after 10 min equilibration. The two ''eyes'' in the upper left are artifacts. The roughening transition occurs between frames (g) and (h). This series of photographs was taken by Yoash Carmi and S. G. Lipson and has not previously been published. Details of the experiments can be found in Ref. 10.

for the hcp system, since to change facets we merely needed to change the appropriate boundary conditions rather than the model details. We report here on simulations of roughening transitions in an hcp crystal with ''ferromagnetic'' ($J_{NN}>0$) nearest neighbor (NN) and both ''ferromagnetic'' ($J_{NNN}>0$) and ''antiferromagnetic'' ($J_{NNN}<0$) next nearest neighbor (NNN) interactions, where J_{NN} and J_{NNN} are the ''exchange'' coefficients for the NN and NNN interactions, respectively. The Hamiltonian is

$$H=-\sum_{\langle NN\rangle} J_{NN}S_iS_j-\sum_{\langle NNN\rangle} J_{NNN}S_iS_j\,. \tag{1.1}$$

A discussion of earlier calculations for the case of positive NNN interactions (J_{NNN}), as well as quantum-mechanical estimates showing that zero point motion may lead to effective negative NNN interactions was given in Ref. 12. Positive higher neighbor interactions led to the prediction of additional and fascinating facets that have never been observed, and did not improve the agreement with the experiment.

While we were carrying out the negative NNN hcp study, experimental results[13] on body-centred-cubic (bcc) ^{3}He were published. Simulations[14] for bcc ^{3}He with NNN interactions in a BCF type of approximation were made and the results were consistent with the measurements, greatly strengthening the idea that lattice models and even BCF-type approximations are reasonable and that reasons (i) or (v) above must be the cause of the discrepancy.

We have also calculated the interface tension as a function of temperature. The results of the Monte Carlo calculation of the interface tension were compared directly to the experimental measurements.[6] As a by-product we measured the bulk order parameter and estimated the critical temperature of the $d=3$ hcp Ising model to be $J_{NN}/K_BT_C\approx 0.10$.

II. MODEL AND METHODS

We studied a three-dimensional (3D) Ising model on an hcp lattice with sample dimensions of $L\times L\times H$ where H is perpendicular to the interface. An interface in the desired direction was imposed either via the use of antiperiodic boundary conditions (APBC), or fixed boundary conditions (FBC). In the former case the uppermost plane was regarded as the lower neighbor of the lowermost plane after all its spins were reversed. In the latter case, the neighbors of the uppermost plane were fixed to point down, while the neighbors of the lowermost plane were fixed to point up. Each up spin ($S_i=+1$) is regarded as a site occupied by a solid atom, and each down spin ($S_i=-1$) as a site occupied by an atom that belongs to the fluid phase. Periodic boundary conditions were applied in the other directions. We sectioned the hcp lattice in the **c**, **a**, and **s** directions. See Fig. 2. In order to ascertain that the crystals had been correctly cut, visualizations of the samples were made. The types of boundary condition errors that occasionally plague development of simulations for cubic systems with higher-neighbor interactions are far more likely to occur in a non-Bravais lattice, and direct visualization proved to be helpful in eliminating these. To facilitate this, and other projects of the Computational Physics group at the Technion, a system of visualization for crystal structures in OpenGL/mesa was developed by Adler

TABLE I. Summary and comparison for the values of T_R calculated from the simulations on the 3D Ising model with the J_{NNN} interaction, the TW calculations (Ref. 11), and those measured by experiments. The results for $J_{NNN}=-0.8$ are obtained via extrapolation of data (see text). The results for positive NNN interaction are after Ref. 12. The temperature units for the simulation is J_{NN}/K_B.

			Our results			
Facet	Expt.	TW	$J_{NNN}=0.0$	$J_{NNN}=0.234$	$J_{NNN}=-0.4$	$J_{NNN}=-0.8$
c	1.28 ± 0.03 K	3.641	4.10 ± 0.01	4.28 ± 0.03	3.77 ± 0.02	3.44
a	≈ 1.0 K	3.39	3.96 ± 0.02	4.15 ± 0.03	3.62 ± 0.03	3.28
ratio **a**/**c**	0.78	0.93	0.96	0.97	0.96	0.95
s	≈ 0.37 K	2.8	3.27 ± 0.02	3.85 ± 0.01	2.00 ± 0.02	0.98
ratio **s**/**c**	0.29	0.77	0.80	0.90	0.53	0.29

and co-workers.[15] The facets in Fig. 2 of the ^{4}He crystal were drawn with this system.

A. Roughening temperatures

In SOS models the interface width is defined as the thermodynamic limit of the height-height correlation function

$$w^2=\lim_{r\to\infty} G(r)=\lim_{r\to\infty}\langle (h_r-h_0)^2\rangle, \tag{2.1}$$

where h_r denotes the height of the surface at the site r, and h_0 is the height at some fixed site. In computer simulations, where sample sizes are finite, the following (equivalent in the thermodynamic limit) quantity is calculated instead

$$w^2(L)=\langle (h_x-\overline{h})^2\rangle, \tag{2.2}$$

where the average is over all lattice sites x. According to KT theory, the squared width of the interface in Eq. (2.2) is finite

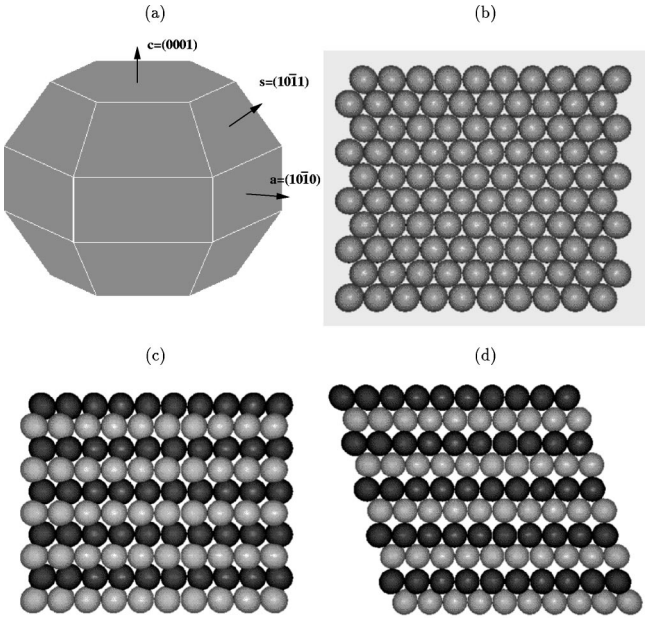

FIG. 2. (a) The geometry of the facets, (b) the **c** facet as viewed from the **c** direction, (c) the **s** facet viewed from the **s** direction, and (d) the **a** facet viewed from the **a** direction. The darker atoms in each plane are displaced in the normal direction to the facet, for the **s** facet by $\sqrt{2/123}a$, and for the **a** facet by $\sqrt{(3)}/6a$, where a is the lattice parameter.

below the roughening transition temperature T_R and diverges logarithmically with sample size L above, with the critical behavior[16]

$$\frac{w^2(L)}{\ln(L)}=\frac{1}{\pi^2}+c_1(T-T_R)^{1/2} \quad \text{for } T>T_R,$$
$$w^2(L)=c_2+(T_R-T)^{-1/2} \quad \text{for } T<T_R, \tag{2.3}$$

where c_1 and c_2 are constants. The width is measured in units of the number of layers (i.e., the number of layers that take part in the interface), not the absolute geometric height of the interface, since the lattice spacing is different in the directions perpendicular to the different interfaces.

In the 3D Ising model, with both types of boundary conditions, the resulting interface contains overhangs and bubbles. It is not pinned by the boundary conditions to a certain equilibrium position but can wander in the sample and is translationally invariant in the direction perpendicular to itself. Because of the overhangs and bubbles, there is no way to define a measure for the interface width unambiguously. However, a generalization of Eq. (2.2) (known as the Gibbs method[17]) for the 3D case consists of assigning a local height h_r to each column perpendicular to the interface by moving all up spins to one end of the column and all down spins to the other end, i.e., the height is equal to the number of solid occupied sites in the column, no matter if they belong to the dense phase, an overhang or a droplet. Then Eq. (2.2) can be applied. The roughening transition is located by fitting the interface width w^2 in the vicinity of the roughening temperature T_R to Eq. (2.3).

B. Surface tension

At zero temperature, the interfacial tension is the excess energy per unit area and is easily calculated for crystal lattices for any direction by enumeration of broken bonds across an interface normal to the surface; a visualization of this is for the case of NNN interactions given in Fig. 3. At finite T the *free* energy of the interface must be calculated. The interfacial excess free energy F_S is defined as the free energy difference between two systems with and without an interface, in which the bulk contributions are identical. This is done by simulating the same system twice, once with antiperiodic (APBC) or fixed (FBC) boundary conditions to produce an interface, and the other with periodic boundary conditions in all directions, which removes the interface. The

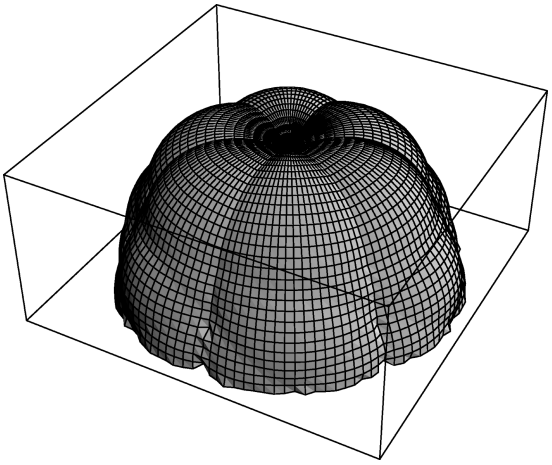

FIG. 3. The Wulff plot at $T=0$ K (Ref. 12).

surface tension γ_S is then obtained by normalizing F_S by the appropriate cross section of area.

In a lattice-gas Monte Carlo simulation one does not have a direct access to the free energy that includes entropy contributions at finite temperatures T. Instead, the free energy is calculated by an integration of the thermodynamic relation

$$\langle E_S \rangle = \frac{\partial(\beta F_S)}{\partial \beta}, \tag{2.4}$$

where $\langle E_S \rangle$ is the thermodynamic average of the internal energy of the interface, and $\beta = 1/T$. Then F_S is given by

$$\beta F_S(\beta) = \int_0^\beta d\beta' E_S(\beta'). \tag{2.5}$$

For a sample of size $L \times L \times H$ the surface tension is given in the thermodynamic limit by

$$\gamma(\beta) = \lim_{L \to \infty} \frac{1}{L^2} F_S. \tag{2.6}$$

III. CALCULATIONS

A. The roughening temperature T_R

The height H of an $L \times L \times H$ sample must be large enough so as not to affect the evolution of the long-wavelength transverse excitations occurring at and above T_R. In simulations on simple cubic lattices[5] it is usually found that a height of $H=10$ is large enough. We have chosen the following three sets of sample sizes: $\{H=10,\ L=10,20\}$, $\{H=20,\ L=6,10,20,40\}$, and $\{H=40,\ L=40,80,160\}$.

In the first set of calculations, we performed simulations on the three facets, **c**, **a**, and **s**, with values of the antiferromagnetic next-nearest-neighbor interaction J_{NNN} in the range $[-0.4,+0.2]$. The reason for choosing negative values for J_{NNN} was discussed in Ref. 12 where it was shown that this may be an implication of quantum interactions. We used a simple spin-flip Metropolis algorithm,[18] with each simulation consisting of 2×10^4 equilibration Monte Carlo steps per site (MCSPS). The interface variance w^2 [Eq. (2.2)], which is a measure of the interface width, was calculated by averaging over 10^4 measurements of it, taken at intervals of 25 MCSPS in order to assure the samples are statistically uncorrelated. Each run was repeated several times for different sets of random numbers and starting configurations. Both APBC and FBC were used. The results for w^2 were equivalent, but there was less statistical noise for the APBC case. Figure 4 shows the resultant interface variance w^2 plotted as a function of temperature T (in units of $J_{NN}/K_B T$), for the **c** facet with different J_{NNN} values. At a fixed T, w^2 increases as J_{NNN} becomes more negative. This is because next-nearest neighbors tend to be antiparallel, hence ''softening'' the interaction and increasing the interface width.

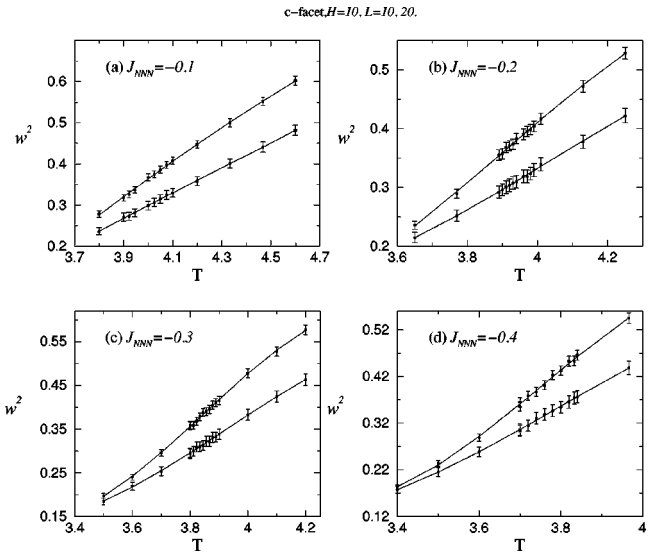

FIG. 4. The interface width squared w^2 as a function of temperature T. Data points are from simulations for the **c** facet, on samples of $L=10$ and 20 and $H=10$ with several negative J_{NNN} values.

In the second set of calculations, we performed simulations on the **s** facet with $H=20$, and $L=6$, 10, 20, and 40. Due to the larger samples used, more effort was required to produce data with an accuracy comparable to that of the smaller samples, hence for $L=40$ the number of MCSPS needed to equilibrate the system was 5×10^4, and the number of MCSPS between two samples of w^2 was 50 MCSPS. Again the mean w^2 was calculated over 10^4 samples. Figure 5 shows w^2 vs $\ln L$ for $J_{NNN}=-0.4$, with some typical error bars. The logarithmic behavior is evident from the good linear fits in the figure, and enables the calculation of $dw^2/d \ln L$.

The roughening transition temperature T_R is estimated by assuming KT theory, and calculating $dw^2/d \ln L$, and then extrapolating to the critical value of $\pi^{-2} \simeq 0.101$ according to Eq. (2.3). Or equivalently, as shown in Fig. 6, the quantity $K_R(T) \equiv (dw^2/d \ln L - \pi^{-2})^2$, may be extrapolated to zero, which in this case gives $T_R^{\mathbf{s}}(J_{NNN}=-0.4)=2.00 \pm 0.05$. Figure 7 shows the slope $dw^2/d \ln L$ as a function of T for several values of J_{NNN} for the **s** facet, while the solid lines are the asymptotic fits based on KT theory according to Eq. (2.3). The good fits reinforce the assumption that the roughening transition is of a KT nature.

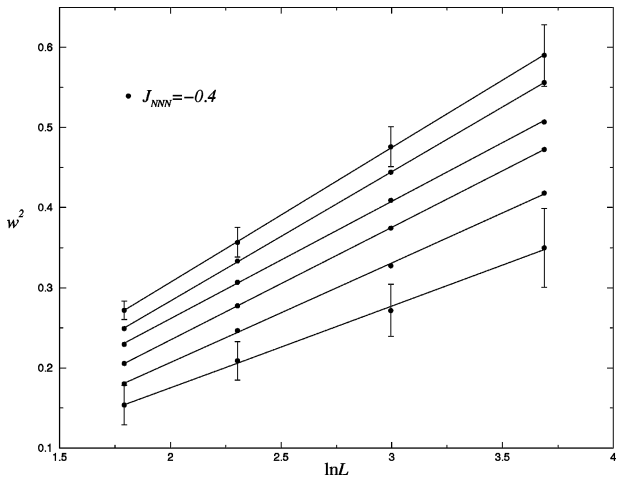

FIG. 5. The interface width squared w^2 as a function of $\ln L$ for different temperatures, from a simulation for the **s** facet on samples of $L=6$, 10, 20, and 40 and $H=20$ with $J_{NNN}=-0.4$. Some typical error bars are shown.

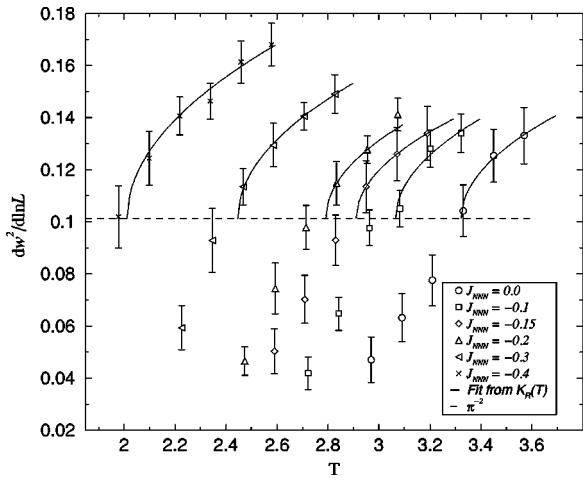

FIG. 7. The slope $dw^2/d\ln L$ plotted as a function of T, from a simulation for the **s** facet on samples of $L=6$, 10, 20, and 40 and $H=20$ with $J_{NNN}=-0.4$. The lines are fits according to KT theory.

We found no substantial difference in estimating T_R for the **s** facet from the simulations with $H=10$, and from those with $H=20$. However, in order to check the effect of finite size samples further, we have performed additional simulations with $J_{NNN}=0.0$ for the **c** facet with $\{H=20,\ L=10,20\}$, where again, as shown in Table II, the results for T_R are equivalent to those of the smaller system with $H=10$ within reasonable error bounds, despite the fact that w^2 is consistently larger in the $H=20$ system.

We further performed a large-scale simulation of samples of size $\{H=40,L=40,80,160\}$ on the **c** facet with $J_{NNN}=0.0$. These simulations were run on the SP2 parallel machine, using a parallel code. Each system was cut into horizontal slices parallel to the facet direction, each slice being of dimension $L\times L\times(H/N)$ where N is the number of nodes. We have achieved an efficiency factor of $\sim$90%, which means that only 10% of CPU time was lost in the communications between the nodes, in our algorithm on 8–16 nodes with sequential spin updates; see details in the Appendix. Each run, depending on the size of the sample, was composed of 30 000–60 000 initial MCSPS to equilibrate the system. The statistical correlation length for these systems with sequential spin updates is large, $\sim$100 MCSPS, but for practical reasons the distance between two samples was 5 MCSPS where the autocorrelation function dropped to $\sim$0.5. The width w^2 was calculated by averaging over 4000 samples. The results from these simulations are shown in Figs. 8 and 9. As predicted by the KT equation (2.3), for $T<T_R$, w^2 is independent of the size L, and diverges with L above T_R. This can be seen from the curve separation in Fig. (8), and in the change in the slope in Fig. (9). The evaluation of T_R is also made by extrapolating the slope to the critical value as before, and is equivalent to that obtained from the smaller systems within an error bound of 5%.

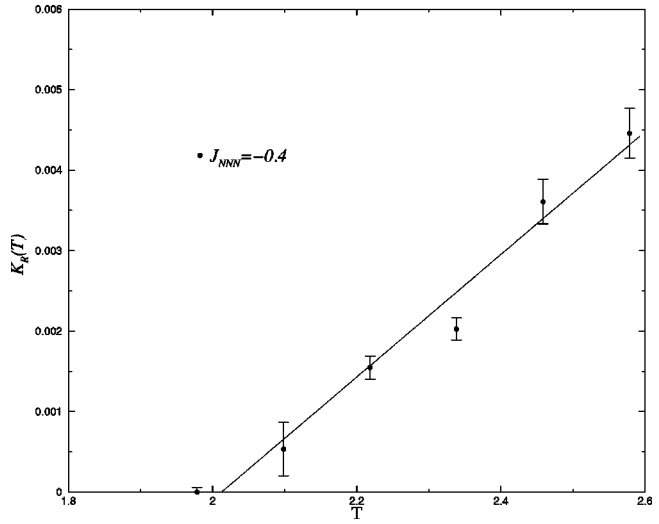

FIG. 6. The quantity $K_R(T)\equiv(dw^2/d\ln L-1/\pi^2)^2$ plotted as a function of T, from a simulation for the **s** facet on samples of $L=6$, 10, 20, and 40 and $H=20$ with $J_{NNN}=-0.4$. The line is a linear fit to the data points.

The results for the roughening temperature T_R as a function of the various NNN interactions are summarized in Table I and plotted in Fig. (10). The results for the **a** and **c** facets are from the first set of simulations with $H=10$, and those for the **s** facet from the second set with $H=20$. The

TABLE II. A comparison of $a(T)\equiv dw^2/d\ln L$ from two simulations of the **c** facet with $H=10$ and $H=20$, and with NN interaction only. From this we determine $T_R=4.1\pm0.05$.

T	$a(T;H=20)$	$a(T;H=10)$
3.5000	0.0117	0.0009
3.6000	0.0053	0.0100
3.7000	0.0058	0.0197
3.8000	0.0223	0.0342
3.9000	0.0401	0.0483
4.0000	0.0691	0.0550
4.1000	0.1075	0.1018
4.2000	0.1150	0.1316
4.3000	0.1101	0.1213
4.4000	0.0974	0.1362
4.5000	0.1418	0.1575

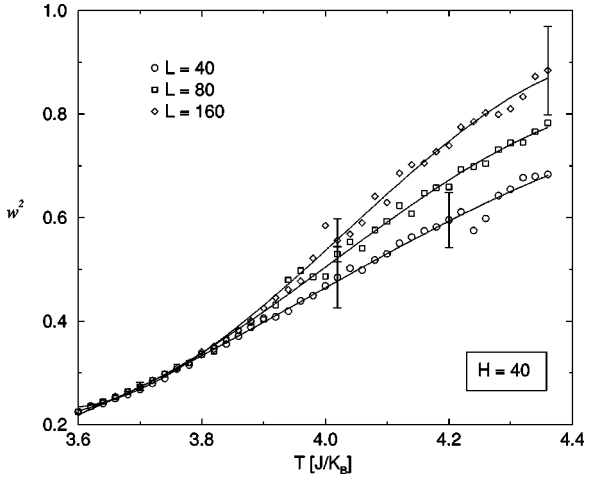

FIG. 8. The interface width $\langle w^2 \rangle$ as a function of temperature T for three **c** facet with height $H=40$ where the width L of each are given in the figure. Some typical error bars are shown.

$\leqslant 5\%$ error bound on T_R, which includes the effect of the size of the system, as well as statistical errors, is shown in the figure. These data are sufficiently precise to clearly show the behavior of T_R vs J_{NNN}.

As shown in Fig. 10 a good linear fit between T_R and J_{NNN} is obtained. The roughening temperature T_R decreases with J_{NNN}; the negative J_{NNN} both increases the range and softens the interaction, which makes it easier to roughen the interface at a given T. Albeit the change in T_R for the **s** facet is faster than in the other directions, this is attributed to the larger number of NNN bonds across the interface in this direction. The correspondence between experimental and calculated ratios of T_R gets better as J_{NNN} decreases. Assuming a linear fit, and by extrapolating, it is possible to obtain an excellent fit at $J_{NNN}=-0.8$. We have not calculated T_R from direct simulations with this value of J_{NNN}. However, to

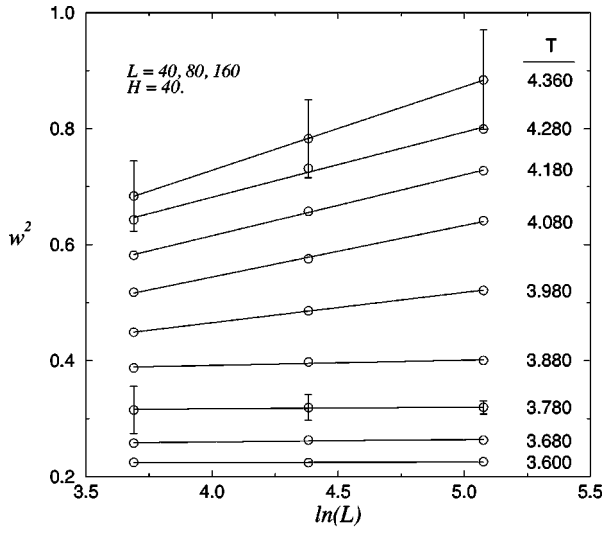

FIG. 9. $\langle w^2 \rangle$ as a function of $\ln L$ for the **c** facet. For low T the slope $dw^2/d\ln L$ is approximately zero, but for high T, $\langle w^2 \rangle$ diverges logarithmically with system size L. Some typical error bars are shown.

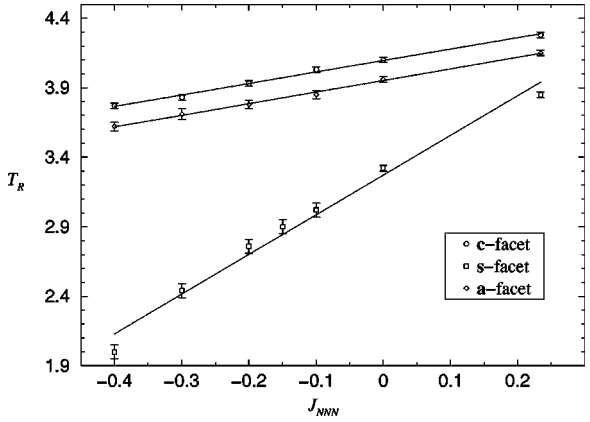

FIG. 10. The roughening temperature T_R vs NNN interaction J_{NNN}.

check whether a stable interface configuration exists under such a relatively large NNN repulsive interaction, we performed preliminary runs up to $J_{NNN}=-1.0$. In all cases stable interfaces were observed.

B. The interfacial tension

For the computation of the interface tension in each of the facet directions **c**, **a**, and **s**, we evaluated the excess surface energy $E_S(T,L)$ as a function of temperature T, and system size L, and substituted in Eqs. (2.5) and (2.6). In addition, the mean bulk order parameter of each sample $M(T,L)$, which by assigning a spin $+1$ to a solid occupied site, and spin -1 to a fluid site, becomes equivalent to the magnetization for a magnetic system, was measured ''for free.'' The temperature was raised in steps of 0.5 in the range $[0.5,15.0]$. Each sample was composed of $L\times L\times L$ spins, where for the **c**-facet samples $\{L=8,10,20,30,60\}$ were used; for the **a** facet $\{L=4,6,8,10\}$ was used, and for the **s** facet, a single system with $\{L=10\}$ was used. The statistical fluctuations in the energy and bulk-order parameter are substantially smaller than those of the interface width, and so a smaller number of Monte Carlo steps was needed, each data point being obtained by sampling over at least 10 000 independent configurations with an error estimate of ~ 0.01.

Each system was simulated twice, once with PBC and once with APBC, with the total energy [Eq. (1.1)] measured in each case. Then $E_S(T,L)$ was estimated from the difference in the energies of the two systems: $E_S=E_{APBC}-E_{PBC}$, where E_{APBC} is the energy of the system with APBC, and E_{APBC} of the PBC system. In all the simulations of this part of the calculations, only NN models were taken, i.e., $J_{NNN}=0$. Figure 11 shows the results for the energy for systems with $L=30$ in the **c** direction under both APBC and PBC. As expected at low T, the energy of the APBC system is larger, and the excess energy due to the interface is shown in the inset. As T increases, the energy of the interface decreases, and the bulk correlation length of the 3D Ising model increases, until it diverges at the bulk critical temperature T_C of the hcp Ising lattice, and smears out any evidence of the existence of the interface. The two systems now have the same energy and E_S drops to zero.[19] The integration over E_S as a function of inverse temperature $\beta=1/K_BT$, as in Eq. (2.5) was carried out by the simple trapezoidal method, start-

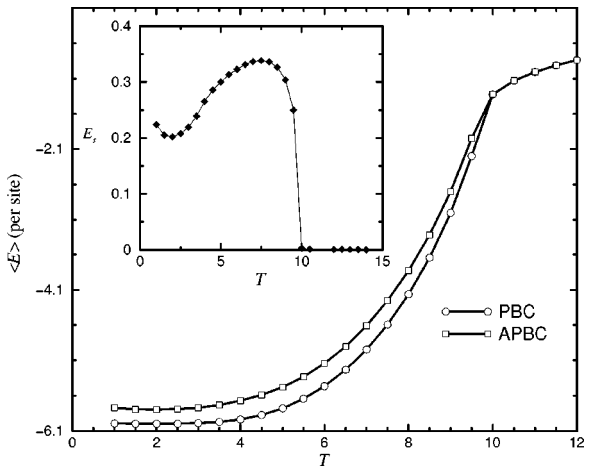

FIG. 11. Energy per site of a system of size $30\times30\times30$, with periodic boundary conditions (PBC), and antiperiodic boundary conditions (APBC), in the direction of the **c** facet as a function of temperature T. The statistical errors of each sample point, in the units of the energy axis, are ~0.01, which is less than the size of the symbols. The inset shows E_S, the excess energy due to the interface. Energy is given in units of J_{NN}.

ing from the highest T down to $T=0.5$. The dependence of F_S on system size squared L^2 was in good agreement with Eq. (2.6) as can be seen from Fig. 12 for the **c** facet. Hence, the data are fit according to the asymptotic behavior $F_S(\beta,L)=\text{const}+\gamma(\beta)L^2$, with the interface tension in the thermodynamic limit given by the slope. The calculated surface tension for the **c** and **a** facets, as well as the results for the **s** facet from one sample with $H=L=10$, are shown in Fig. 13. The interface free energy at $T=0$ is equivalent to the interface excess free energy and can be calculated exactly from the ground state of each system, and its value turns out to be in good agreement with that calculated at $T=0.5$, as can be seen in Fig. 13.

The results of our Monte Carlo calculations for the interface tension may be directly compared to the experimental

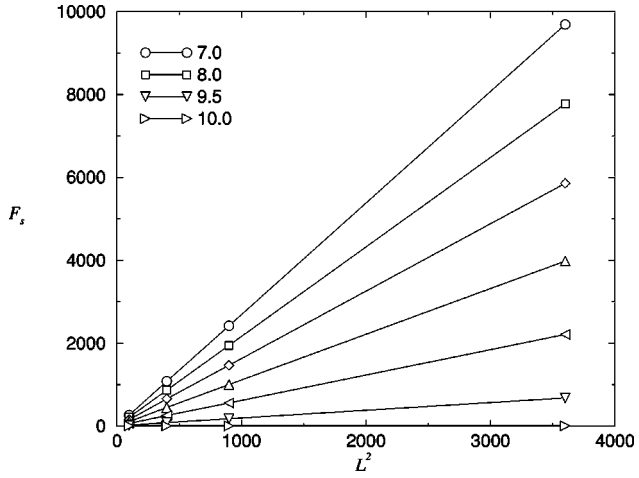

FIG. 12. The interfacial excess free energy F_S as a function of L^2 for various temperatures as indicated. This enables extraction of the normalized surface tension, given by the slopes of the lines [from Eq. (2.6)].

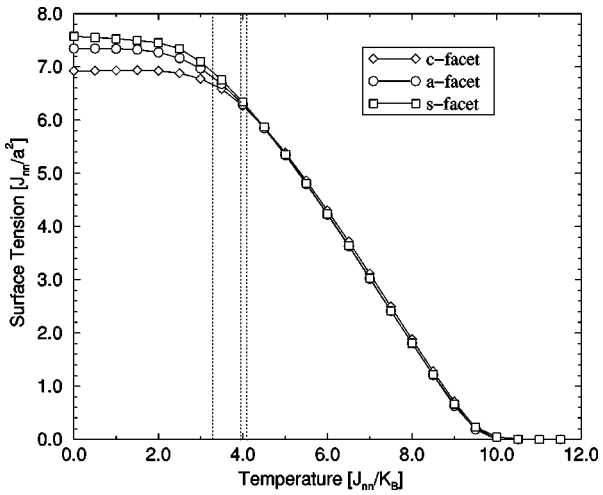

FIG. 13. Comparison of the interface tension for the three facets as a function of temperature T.

measurements of the interface tension,[6] by transforming the units of the simulations. In the simulation, the units of the temperature are given by $[J_{NN}/K_B]$, with the Boltzmann constant being $K_B\approx1.38\times10^{-16}$ erg/K. In these units, the calculated roughening temperature of the **c** facet with NN interaction only[20,12] is $T_R=4.10J_{NN}/K_B$, while experimentally[6,7] $T_R=1.28$ K. A direct comparison then gives

$$T^{\mathbf{c}}_{R,NN}=4.10\frac{J_{NN}}{K_B}=1.28\ \text{K}\Leftrightarrow\frac{J_{NN}}{K_B}=0.3121\ \text{K}. \quad (3.1)$$

On the other hand, the unit of the interface tension in the simulations is given by J_{NN}/a^2, where a is the NN distance. For solid helium on the coexistence line at $T\approx1.0$ K, and pressure 25 atm, the measured spacing is $a=3.7$ Å.[21] Hence, by using the value of J_{NN} from Eq. (3.1), we obtain the calculated interface tension in terms of the physical units erg/cm^2. In Fig. 14 the computed interface tension for the **c** facet is plotted together with experimental measurements of Ref. 6. We can see that despite the simplicity of the model, a fairly good agreement is achieved, although the computed surface tension is consistently larger than the measured one, which can possibly be attributed to the neglect of various relaxational effects on the surface that lead to the reduction of the surface tension. Clearly negative NNN interactions would reduce the calculated surface tension and also improve the fit.

C. The ''magnetization'' and T_C of the hcp Ising model

Although in most of our simulations we were primarily interested in the temperature region near T_R, the simulations of the interfacial energy extended up to the bulk critical temperature T_C of the 3D Ising system. During these simulations in addition to calculating the energy as a function of temperature and system size, we have also calculated (''for free'') the bulk order parameter, or simply the magnetization

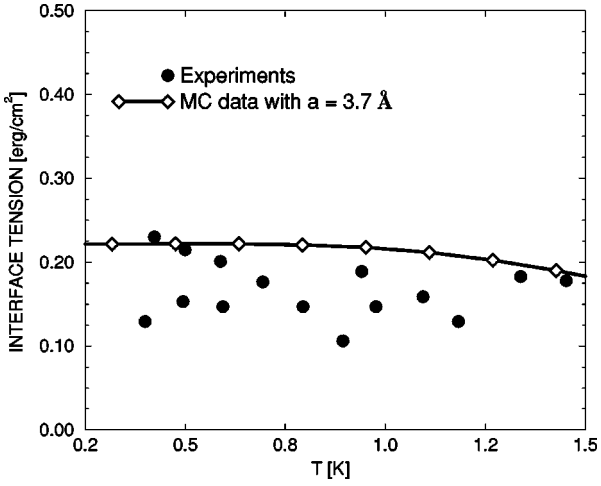

FIG. 14. Comparison between experiments (Ref. 6) and simulations of the interface tension for the **c**-facet with NN interaction only. The size of the system is $10\times10\times10$, and the integration starts at $T=0$ K.

in a magnetic system: $M(L,T)=\Sigma_i S_i/(L^3)$, which is the average spin at a site. A look at $M(L,T)$ plotted in Fig. 15 as a function of temperature for the **c** facet reveals an interesting behavior for M in the APBC system during roughening. For the system with PBC, M behaves as expected starting from unity and going down to zero as $T\rightarrow T_C$, while in the APBC system, for $T\leqslant T_R$, $M\simeq 0$ because of the interface, but close to the roughening region, large fluctuations appear that are due to the surface being delocalized and hence can wander to either side of the sample during the simulation, introducing large fluctuations to the bulk order parameter.

At T_C itself, as we have mentioned earlier, the effect of the boundary conditions is lost and the bulk order parameter is zero. From these bulk order parameter results we estimate the location of T_C for the 3D Ising model on an hcp lattice to be $J_{NN}/K_BT_C\approx 0.10$, compared to $J_{NN}/K_BT_C\approx 0.221\,659$ of the simple cubic Ising model,[23] and 0.08 for 12 neighbors in mean-field theory. Our data are not accurate enough in this region to enable a good check of the universality of the critical exponent of the magnetization.

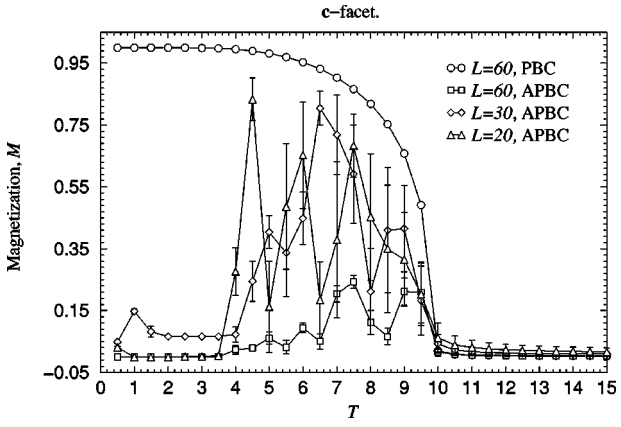

FIG. 15. The bulk order parameter calculated from the PBC and the APBC systems in the **c** facet direction.

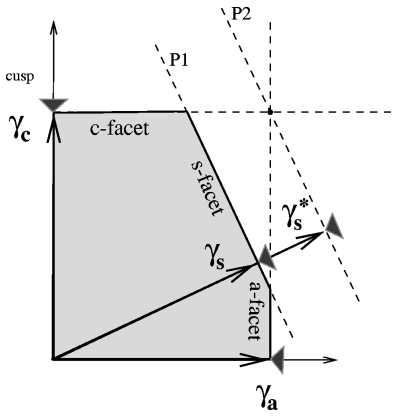

FIG. 16. A schematic description of a planar projection of the γ plot perpendicular to the **c** facet and passing through the **a** and **s** facets. The angle is approximately $\theta\simeq 27.93$, (see text).

D. Thermal faceting?

As mentioned in the Introduction, one of the motivations for this work was the large observed discrepancy between experiments and simulations of lattice models concerning the roughening temperature of the **s** facet. An explanation that can be discussed in terms of the calculations is that there is an effective large negative NNN interaction between the atoms, but although we have considered[12] a quantum origin for this interaction, recent investigations[24] do not support this conjecture. It is therefore worthwhile looking for an alternative explanation.

Computing the equilibrium crystal shape of an hcp lattice with NN interaction only at $T=0$ K (Ref. 12) showed that there are only three cusps in the Wulff plot corresponding to the three known facets, namely, **a**, **c**, and **s**. As temperature increases, these cusps weaken, and eventually fade out at their corresponding roughening temperatures. It is reasonable to assume that these cusps remain the only shape-decisive features, since as T increases the surface tends to roughen, and cusps fade away, hence no new cusps are likley to emerge at $T>0$, if they are not evident already at $T=0$. Thus the calculation of the surface tension of the three facets provides a picture of the evolution of the equilibrium crystal shape as a function of temperature. The three facets **c**, **a**, and **s** lie in the same crystallographic zone (i.e., have normals in the same plane), and it is possible that one of them (**s** in our case) may not appear on the equilibrium crystal shape if the total surface energy can be reduced by replacing it by the other two (**a** and **c**). A flat surface (not a facet) in the **s** direction would then appear microscopically to have alternating facets in the **a** and **c** directions; this is called ''thermal faceting'' and has been discussed by Rottman and Wortis.[25,26] On the Wulff plot, this seems to be energetically favorable if the plane representing the **s** facet lies outside the rectangle of planes representing the **a** and **c** facets (Fig. 16) and we denote the required value of γ_s for this to occur by γ_s^*. Since γ_c, γ_a, and γ_s are functions of T, it is possible that this condition arises at some temperature T_t below the roughening temperature of the **s** facet, and so the **s** facet would only appear below T_t. This temperature would there-

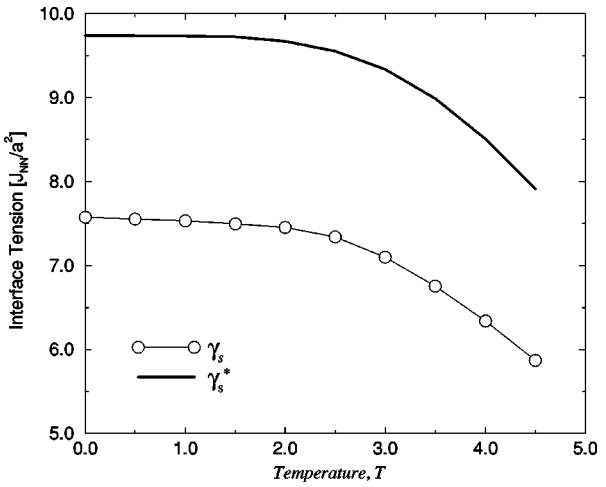

FIG. 17. Surface tension γ_s of the **s** facet obtained from the simulations with NN interactions, and the threshold values γ_s^* above which the **s** facet becomes unstable.

fore be identified erroneously as the roughening temperature of the **s** facet in an experiment. For the hcp geometry, this condition translates to

$$\gamma_s \geqslant \gamma_s^* \equiv \frac{\sqrt{9}\,\gamma_C + \sqrt{32}\,\gamma_a}{\sqrt{41}}. \tag{3.2}$$

In Fig. 17, the value of γ_s^* as a function of T, calculated from the values of γ_c and γ_a according to Eq. (3.2), is plotted along with the calculated γ_s. Obviously, there is no indication of thermal faceting, so the question remains open.

IV. CONCLUSIONS

We have applied techniques well established on cubic lattice models for calculating the equilibrium roughening temperature, and the temperature dependence of the interface tension to a real non-Bravais lattice, with both NN and NNN interactions. The comparison of the interface tension between theory and experiment shows that even the NN model is quite close to the reality, although there is still room for improvement of some details. Qualitative agreement between experiment and simulation is found in the case of the **a** and **c** facets for T_R (as was also found by TW.) This was not the case for ratios involving the **s**-facet in TW. However, once the NNN interactions are included, in particular, the negative ones as reported in Table I, we see that for $J_{NNN}/J_{NN} \leqslant 0.4$ reasonable agreement for the **c/s** ratio is obtained. It is possible to obtain a ''best fit'' between the calculations and experiments for $J_{NNN}/J_{NN} = -0.8$ (see Table I). However we are not certain that J_{NNN}/J_{NN} as high as 0.8 is entirely reasonable, although it does indeed provide a good fit. Thus we can clear up the discrepancy between theory and experiment only at a price we are uncertain whether it is reasonable to pay.

The large value of the higher neighbor interaction suggests that perhaps we should have carried out calculations for third and even higher neighbor interactions. There are a number of ways that third and higher-neighbor interactions of different strengths and signs could sum to an effective value of 0.8 while each was more reasonable in magnitude. However, such a study would be somewhat involved without adding much to our general conclusions, and therefore was not pursued at this stage.

Let us now review the list of reasons given in the Introduction to explain the disagreement between theory and experiment regarding $T_R^{\mathbf{s}}$ and see which have been overcome. By including both positive and negative higher neighbor interactions we have shown that (i) lack of higher-neighbor interactions was definitely a problem. The next point, (ii) lack of quantum effects by TW, is also relevant from the viewpoint[12] that Gemintern *et al.*[14] show that a likely result of quantum effects is the negative NNN interaction. The point (iii), problems with the BCF approximation, is less relevant as the results of the full model and the BCF ones where avaliable for comparison are not so different numerically. Given the overall success for both the surface tension and T_R measurements here and in Ref. 14 we suggest that any corrections obtained by removing the lattice constraint, point (iv) in the list, will be a higher-order effect.

However, since we do need the very large NNN interactions to provide agreement with experiment, item (v), lack of equilibration in the experiments during faceting of the **s** facet, is still a possibility. There were earlier claims that the measured value may be strongly influenced by the nonequilibrium conditions under which the experiments were made. We think that future progress on this problem must come in the experimental context.

ACKNOWLEDGMENTS

Support of the Israel Science Foundation was essential for both the experimental and simulational aspects of this project. We acknowledge the Technion Visualization Center (and advice from B. Peri), Minerva Non-Linear Center, and the Israeli Inter University High Performance Computing Center for support for the visualization and simulation. We thank D. Stauffer for advice on aspects of the simulations, and Y. Carmi and A. Gemintern for their earlier collaboration on this project.

APPENDIX: PARALLEL ALGORITHM

To parallelize the calculations for the SP2, the sample was divided into slices parallel to the interface. Each slice was handed to a single processor or node, were it would then be treated separately. The initial condition was set to the ground state of each system: all up (or down) spins for PBC and upper half up/lower half down of the APBC cases. Spins were updated sequentially, starting from the lower layer of spins in each node. Since the lower layer of node i is the NN layer of the top layer of node $i-1$, the spins from this layer should be copied to the bottom layer, with spin inversion for the uppermost and lowermost slices in the APBC case. Care must be taken in updating the boundary conditions, so as not to update a layer in a certain step before its neighbors from another node were copied in the *same* step.

[1] W. K. Burton, N. Cabrera, and F. C. Frank, Philos. Trans. R. Soc. **243**, 299 (1951).
[2] H. Van Beijeren, Commun. Math. Phys. **40**, 1 (1975).
[3] S. T. Chui and J. D. Weeks, Phys. Rev. Lett. **40**, 733 (1978).
[4] M. Hasenbuch, M. Marcu, and K. Pinn, Physica A **208**, 208 (1994).
[5] M. Hasenbuch and K. Pinn, Physica A **203**, 189 (1994).
[6] J. Landau, S. G. Lipson, L. M. Maatanen, L. S. Balfour, and D. O. Edwards, Phys. Rev. Lett. **45**, 31 (1980).
[7] K. O. Keshishev, A. Ya. Parshin, and A. V. Babkin, Zh. Eksp. Teor. Fiz. **80**, 716 (1981) [Sov. Phys. JETP **53**, 362 (1981)].
[8] J. E. Avron, L. S. Balfour, C. G. Kuper, J. Landau, S. G. Lipson, and L. S. Schulman, Phys. Rev. Lett. **45**, 814 (1980).
[9] P. E. Wolf, S. Balibar, and F. Gallet, Phys. Rev. Lett. **51**, 1366 (1983).
[10] Yoash Carmi (private communication).
[11] M. Touzani and M. Wortis, Phys. Rev. B **36**, 3598 (1987).
[12] S. G. Lipson, J. Adler, G. Baum, A. Gemintern, and A. Hashibon, J. Low Temp. Phys. **101**, 683 (1995).
[13] R. Wagner, S. C. Steel, O. A. Andreeva, R. Jochemsen, and G. Frossati, Phys. Rev. Lett. **76**, 263 (1996).
[14] A. Gemintern, S. G. Lipson, and J. Adler, Phys. Rev. B **55**, 15 441 (1997).
[15] J. Adler, *Proceedings of the Scientific Visualization Conference* (Hebrew University, Jerusalem, 1995), p. 59; J. Adler, A. Hashibon, A. Kanigel, I. Rosenblum, and D. Saada, in Recent Developments in Computer Simulation Studies in Condensed Matter Physics, XI, edited by D. Landau and B. Schuttler (Springer, Berlin, in press).
[16] J. M. Kosterlitz and D. J. Thouless, J. Phys. C **6**, 1181 (1973); J. K. Kosterlitz, *ibid.* **7**, 1046 (1977); T. Ohta and K. Kawasaki, Prog. Theor. Phys. **60**, 365 (1978); K. K. Mon, D. P. Landau, and D. Stauffer, Phys. Rev. B **42**, 545 (1990).
[17] S. Kremer and D. Wolf, Physica A **182**, 542 (1992).
[18] K. Binder and D. W. Heermann, *Monte Carlo Simulations in Statistical Physics*, Springer-Verlag Series in Solid State Physics (Springer-Verlag, Berlin, 1992), and references therein; N. Metropolis, A. W. Rosenbluth, M. N. Rosenbluth, A. H. Teller, and E. Teller, J. Chem. Phys. **21**, 1087 (1953); J. J. Binney, N. J. Dowrick, A. J. Fisher, and M. E. J. Newman, *The Theory of Critical Phenomena* (Clarendon Press, Oxford, 1992).
[19] Strictly speaking, there is no critical point between a solid and a liquid or vapor, but for the Ising model approximation such a point exists.
[20] Gideon Baum, MSc thesis, Technion, 1994.
[21] Fritz London, *Superfluids*, 2nd ed. (Dover, New York, 1964); and also W. G. Wyckoff, *Crystal Structure* (Interscience, New York, 1963), Vol. 1, pp. 11, 13, and 56; See also C. A. Swenson, Phys. Rev. **79**, 626 (1950), where a is calculated from the molar volume (see Ref. 22).
[22] S. G. Lipson, Contemp. Phys. **28**, 117 (1987), and references therein.
[23] Z. Salman and J. Adler, Int. J. Mod. Phys. C **9**, 195 (1998).
[24] A. Gemintern (private communication).
[25] C. Rottman and M. Wortis, Phys. Rep. **103**, 59 (1984).
[26] C. Herring, in *Structure and Properties of Solid Surfaces*, edited by R. Gomer and G. S. Smith (Univ. of Chicago Press, Chicago, 1955).